Available online at www.sciencedirect.com
SCIENCE DIRECT®
Journal of Power Sources 145 (2005) 407–415
JOURNAL OF POWER SOURCES
www.elsevier.com/locate/jpowsour

Statistic analysis of operational influences on the cold start behaviour of PEM fuel cells

M. Oszcipok*, D. Riemann, U. Kronenwett, M. Kreideweis, M. Zedda

Fraunhofer Institute for Solar Energy Systems, Germany

Accepted 2 February 2005
Available online 29 April 2005

Abstract

For portable fuel cell systems a multitude of applications have been presented over the past few years. Most of these applications were developed for indoor use, and not optimised for outdoor conditions. The key problem concerning this case is the cold start ability of the polymer electrolyte membrane fuel cell (PEMFC). This topic was first investigated by the automotive industry, which has the same requirements for alternative traction systems as for conventional combustion engines.

The technical challenge is the fact that produced water freezes to ice after shut-down of the PEMFC and during start-up when the temperature is below 0 °C.

To investigate the basic cold start behaviour isothermal, potentiostatic single cell experiments were performed and the results are presented.

The cold start behaviour is evaluated using the calculated cumulated charge transfer through the membrane which directly corresponds with the amount of produced water in the PEMFC. The charge transfer curves were mathematically fitted to obtain only three parameters describing the cold start-up with the cumulated charge transfer density and the results are analysed using the statistical software Cornerstone 4.0.

The results of the statistic regression analyses are used to establish a statistic-based prediction model of the cold start behaviour which describes the behaviour of the current density during the experiment. The regression shows that the initial start current mainly depends on the membrane humidity and the operation voltage. After the membrane humidity has reached its maximum, the current density drops down to zero. The current decay also depends on the constant gas flows of the reactant gases.

Ionic conductivity of the membrane and charge transfer resistance were investigated by a series of ac impedance spectra during potentiostatic operation of the single cell at freezing temperatures. Cyclic voltammetry and polarisation curves between cold start experiments show degradation effects by ice formation in the porous structures which lead to significant performance loss.

Keywords: PEMFC; Cold start; Statistic analysis; Impedance spectroscopy; Cyclic voltammetry; Degradation

1. Introduction

Sub zero temperature operation of portable fuel cell systems is a relatively new topic and not much literature is published. Cargnelli et al. operated a 50 W PEMFC system in a climatic chamber at −42 °C and used for the start-up a catalytic burner to heat up and humidify the reaction air [1]. Chu et al. operated a 50 W fuel cell system at −10 °C for 9 h [2]. Datta and Velayutham reports of a 500 W fuel cell system which was operated without any problems in the Antarctic [3].

More fundamental in situ investigations of non-isothermal, galvanostatic single fuel cell experiments below 0 °C were performed by Kagami et al. At constant gas flow it is described that the cathode electrode surface is reduced by ice formation and therefore the reaction is inhibited. With the empirical assumption that the cathode surface is diminished proportional with the amount of frozen water, simulations were done which describe the voltage decay over time in

* Corresponding author. Tel.: +49 761 4588 5432; fax: +49 761 4588 9432.
E-mail address: michael.oszcipok@ise.fraunhofer.de (M. Oszcipok).

0378-7753/$ – see front matter © 2005 Elsevier B.V. All rights reserved.
doi:10.1016/j.jpowsour.2005.02.058

Nomenclature

BET	Brunauer–Emmett–Teller porosity analysis
c	exponent variable, constant
CV	cyclic voltammetry
EDS	energy dispersive X-ray spectroscopy
F	Faraday constant (96485 C mol^{-1})
GDL	gas diffusion layer
i	current density (mA cm^{-2})
$i_{\text{linear,start}}$	current density at start of slow decrease (mA cm^{-2})
i_{peak}	peak current density during cold start (mA cm^{-2})
i_{start}	current density at initial cold start (mA cm^{-2})
MEA	membrane electrode assembly
$m_{\text{H}_2\text{O,prod}}$	area specific product water (g cm^{-2})
$M_{\text{H}_2\text{O}}$	molar weight of water (g mol^{-1})
MPL	microporous layer between electrode/GDL
p	influence parameter in regression polynomial
p_{450}	reference power density at 450 mV (mW cm^{-2})
R^2	stability index
R^2_{adj}	adjusted stability index
R_{ct}	charge transfer resistance from Nyquist plot (mΩ cm^2)
$R_{\text{m,c}}$	membrane/contact resistance from Nyquist plot (mΩ cm^2)
SEM	scanning electron microscopy
$S_{\text{q,cum}}(t)$	cumulated charge transfer density (C cm^{-2})
$S_{\text{q,fit}}$	fitted cumulated charge transfer density (mC cm^{-2})
$S_{\text{q,max}}(t)$	max. cumulated charge transfer density (C cm^{-2})
$S_{\text{q,peak,end}}$	cum. charge transfer density at end of peak (mC cm^{-2})
$S_{\text{q,peak,start}}$	cum. charge transfer density at start of peak (mC cm^{-2})
t_{63}	time when $S_{\text{q,fit}}(t)$ reaches 63% of $S_{\text{q,max}}$ (min)
u_{air}	air flow rate (ml min^{-1})
V	voltage (mV)
V_{OC}	open circuit voltage (mV)
x_{i}	value of influence parameter
y	response variable in regression polynomial
Z_{start}	Impedance at 1000 Hz before cold start-up (mΩ)

good correlation with experimental results. Beneficial for the cold starts are low current densities which prevent voltage decay by freezing of product water [4,5].

In this paper we present the results of potentiostatic single cell cold start-up measurements under isothermal conditions at −10 °C. The current density is increasing very fast after initial start-up and later it decays towards zero. This behaviour is ascribed to freezing of product water in the cathode. To find out the main influencing operational parameters on the cold start behaviour, statistic methods are used. Finally, a statistic-based prediction model of the current decay during isothermal cold start was developed.

To get a deeper insight into the dynamic processes in the cathode during cold start-up dynamic electrochemical impedance spectroscopic analyses were done, which show that the membrane/contact resistance as well as the charge transfer resistance is changing with the amount of produced water.

Impedance spectroscopy at 80 °C was also used by Cho et al. to find out changes of single fuel cell characteristics by ex situ thermal cycling. The author concludes that the contact resistance in the fuel cell is increasing after thermal cycles because of worse contact between the membrane and the electrode, whereas the membrane ionic conductivity itself is not affected [6]. The impact of ex situ thermal cycling on the degradation of Nafion® membranes was examined by McDonald et al. It is reported that the ionic conductivity and the mechanical properties are hardly changing. However, opening up of the molecular structure of the polymer in connection with enlargement of hydrophilic areas was found [7]. Cappadonia et al. investigated Nafion® membranes by thermal cycling and it was found that two different water environments exist below 0 °C. Water phase transition depends on the water content in the membrane. Higher water contents lead to larger pore diameters in the membrane and therefore to a lower freezing temperature of water. In water-rich samples phase transitions were observed at 260 K [8].

Nevertheless, performance degradation can be observed, as described in [6,9]. A degradation rate of about 2.8% at 80 °C and 0.6 V per-freeze-thaw cycle down to −10 °C is observed as well as a reduction of about 6% per thermal cycle of the electrochemical active surface area of the cathode. It was found that the pore size distribution in the electrode changes to larger pores by thermal cycles.

Our measurements with cylic voltammetry (CV) also show degradation of the cathode electrode surface by isothermal sub zero operation, and furthermore changes in hydrophobicity of both, the microporous layer (MPL) and the gas diffusion layer (GDL) on the cathode side. We finally also found performance degradation at 450 mV and 30 °C of more than 5% per each cold start experiment.

2. Experimental and results

2.1. Maximum cumulated charge transfer density

The cold start experiments were carried out with a single cell with an active area of 46 cm^2. The flowfield had a double serpentine structure and the cell assembly was done using commercial standard components consisting of GDL, MPL and catalyst-coated membrane.

Before freezing the fuel cell a reference performance measurement at 450 mV with dry hydrogen (stoichiometry 1.5) and dry air (stoichiometry 3.0) at 30 °C was recorded. This reference power density is called p_{450}. Each reference point was measured at least 20 min whereby gas flows were adjusted automatically to the actual current.

After this reference operation the gases were switched to dry nitrogen (N_2), and the anodic as well as the cathodic side of the fuel cell were purged with 1.0 l min^{-1} at 30 °C. The purging process continued until the high frequency resistance at 1000 Hz increased by a factor of about 100 and more. Then, N_2 flow was switched off and the cell was cooled down.

After drying and freezing of the cell, the start-up experiments were carried out potentiostatically. Gas flow rates as well as the cell temperature were kept constant. The dew point temperatures of the gases are between −10 °C and −5 °C. When the graphite plates reach the required temperature, dry hydrogen and dry air are switched on. After open circuit voltage has arisen, potentiostatic load is applied and the current over time is recorded. For evaluation of the cold start experiments, the cumulated charge transfer density $S_{q,cum}(t)$ serves, which is calculated by (1).

$$S_{q,cum}(t) = \int_0^t i\,dt \tag{1}$$

$S_{q,cum}(t)$ integrates over the dynamic current density and it directly correlates with the amount of product water $m_{H_2O,prod}$, given by Eq. (2).

$$m_{H_2O} = \frac{S_{q,cum}(t)}{2F} M_{H_2O} \tag{2}$$

To find out the main influencing operating parameters 15 experiments were carried out at constant temperature of −10 °C. In Table 1, all varied operational parameters are listed.

After the fuel cell is dried out, cooled down to −10 °C and V_{OC} has arisen, potentiostatic load is applied. The resulting current reacts over time always with the same principle behaviour, that is a fast increase which reaches within the first 2 min its maximum and then decays towards zero. To predict the maximum cumulated charge transfer density $S_{q,max}$, a mathematical fitting function was found which parameterises $S_{q,cum}(t)$. This exponential function is calculated by (3).

$$S_{q,fit}(t) = S_{q,max}(1 - e^{-(t/t_{63})^c}) \tag{3}$$

The quality of a cold start experiment is evaluated by $S_{q,max}$. A linear regression analysis was performed to predict the main influencing operational parameters on $S_{q,max}$ using the statistic software Cornerstone® (Brooks Automation). It fits a response y, e.g. $S_{q,max}$, with a polynomial term consisting of a constant c; the values x_i of the p influence parameters, e.g. applied voltage V, multiplied by constant factors a_i. In (4), a general polynomial equation is shown where linear effects are taken into account ($a_i\,x_i$), interaction effects between each parameter ($a_{ij}\,x_{ij}$) and quadratic effects ($a_{ii}\,{x_i}^2$).

$$y = c + \sum_{i=1}^{p} a_i x_i + \sum_{i,j=1,i\neq j}^{p} a_{ij} x_{ij} + \sum_{i=1}^{p} a_{ii} {x_i}^2 \tag{4}$$

The fit quality of the regression polynomial is evaluated by the stability index R^2 and the adjusted stability index R^2_{adj}. R^2 is the relation between the statistical spread of the model and the statistical spread of the real measured values. For test series with a low number of experiments R^2_{adj} is better suited, because it accounts additionally for the number of experiments and the number of influence parameters. The values of R^2 and R^2_{adj} are between 0 and 1. For significant regression model the stability index should be near one [13]. Using the calculated polynomial which represents the regression model, it is possible to predict $S_{q,max}$ within the regression boundaries.

Fig. 1 illustrates the regression result for $S_{q,max}$ as predicted response graph. Three parameters were found which have a significant impact on the value of $S_{q,max}$. The largest effect has the reference power density $p_{450,}$ which depends on the degree of degradation. The influence of the air flow rate u_{air} and the membrane humidity indicated by Z_{start} is lower. The coefficient correlation between these three parameters is lower than 0.4, which indicates that they are independent. On the y-axis the predicted response from the linear regression polynomial is shown as the function of the values of p_{450} (here adjusted to 250 mW cm^{-2}), u_{air} (600 ml min^{-1}) and Z_{start} (40 mΩ). The predicted value for $S_{q,max}$ is 47.99 C cm^{-2} with a standard deviation of ±12.9 C cm^{-2}.

This regression result indicates that two operational parameters can be adjusted by the operator to achieve a high charge transfer below 0 °C. The membrane should be dry, indicated by a high Z_{start} and the air flow rate should be also as high as possible. The third and most strongly influencing parameter is the overall performance parameter p_{450}. With

Table 1
Varied operating parameters for start-up experiments at −10 °C

Operating parameter	Symbol/unit	Values
Applied voltage for cold start-up	V/mV	200/400/600
Air flow rate	u_{air}/ml min^{-1}	147–1000
Hydrogen flow rate	u_{H_2}/ml min^{-1}	20–158
Cell impedance after nitrogen purging	$Z_{purging}$/mΩ	70–1500
Cell impedance after applying gases, directly before cold start	Z_{start}/mΩ	7–50
Power density at 450 mV, 30 °C, dry gases, stoichiomety 1.5/3.0	p_{450}/mW cm^{-2}	210–350

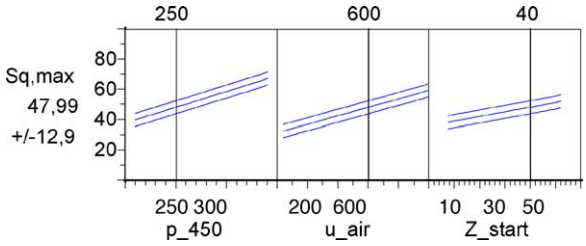

Fig. 1. Predicted $S_{q,max}$ as function of the dominating three operational parameters. Linear regression of all operational parameters ($R^2_{adj} = 0.87$).

higher performance the local electrode temperature is higher [10] and it is assumed that crystallisation of water starts in the more distant areas of the GDL and not immediately in the electrode. Therefore, a longer operation is possible before ice formation hinders the reaction.

2.2. Current decay

To analyse the initial starting behaviour at −10 °C the current density i is referred to the cumulated charge transfer density $S_{q,cum}(t)$. For statistical evaluation it is necessary to parameterise these current density curves, which is done by taking five characteristic curve points into account.

To find out which operational parameters affect the shape of the current decay curve, linear regression analyses were made for each point. Interactions of the main parameters (V, u_{air}, u_{H_2}, Z_{start}, p_{450}) are included. The goodness of the regression analysis is indicated by R^2_{adj} which is for all points between 0.855 and 0.998, except for point 5 ($S_{q,max}$), where R^2_{adj} is 0.640. Table 2 shows all coefficients for the statistic prediction polynomial.

As an example the regression model calculates $S_{q,linear}$ (Point 4) with a polynomial expression given by the constant c and coefficients multiplied by the adjusted values of the influence parameter, in this example u_{air} and Z_{start}:

$$S_{q,linear} = 3.9557 - 0.0024u_{air} + 0.4184Z_{start} + 0.0004u_{air}Z_{start}$$

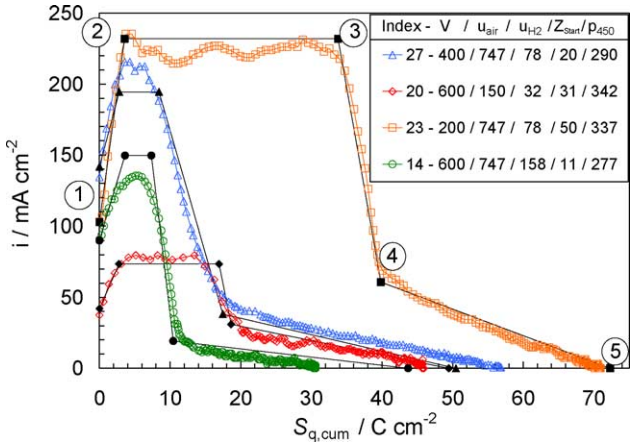

Fig. 2. Statistical based fit of current decay curves at −10 °C and different operating conditions as shown in legend. Experimental data are indicated with open symbols (△, ◊, □, ◯) and the belonging statistical 5-point fit with filled symbols (▲, ♦, ■, ●).

In Fig. 2, four experimental results for the current density over the charge transfer density for different operating conditions are shown. Additionally, the fitting curves of the above-introduced statistical 5-point fitting model are included. This demonstrates that it is possible to describe the current density decay over the cumulated charge transfer density by the operational parameters.

The statistic-based model estimates the dominating factors for each curve point. In Table 3, the percentage influence is shown.

The regression shows that the initial start current i_{start} mainly depends on the membrane humidity Z_{start} and the

Table 2
Coefficients for polynomial prediction model

Point	①	②/③			④		⑤
	i_{start} (mA cm^{-2})	$S_{q,peak,start}$ (mA cm^{-2})	i_{peak} (mA cm^{-2})	$S_{q,peak,end}$ (mA cm^{-2})	$S_{q,linear}$ (C cm^{-2})	i_{linear} (mA cm^{-2})	$S_{q,max}$ (mA cm^{-2})
c	−977.8981	−22.4874	144.9494	7.4862	3.9557	−1.9906	−26.0127
V	2.9383		−0.2209	−0.0180		−0.0056	
u_{air}	0.9819	0.0229	−0.4419	0.0104	−0.0024	0.0582	0.0247
u_{H_2}		0.6911		−0.6934			
Z_{start}	−36.3194	0.3027	−3.1301	0.3954	0.4184		0.4772
p_{450}	3.8487		0.1402			0.1094	0.1663
$u_{air}u_{H_2}$		−0.0008					
Vu_{air}	−0.0014					−0.0001	
VZ_{start}	0.0158		0.0036				
$p_{450}V$	−0.0104						
$u_{H_2}Z_{start}$		−0.0078		0.0107			
$u_{air}Z_{start}$	−0.0123	0.0004			0.0004		
$p_{450}u_{air}$			0.0021				
$p_{450} \times Z_{start}$	0.0888						
Uu_{H_2}				0.0009			

Table 3
Estimated influence of main parameters on current decay curves

Point	①	②/③			④		⑤
	i_{start}	$S_{q,peak,start}$	i_{peak}	$S_{q,peak,end}$	$S_{q,linear,start}$	$i_{linear,start}$	$S_{q,max}$
V	34%	–	40%	25%	–	59%	–
u_{air}	19%	68%	92%	5%	13%	20%	5%
u_{H_2}	–	69%	–	4%	–	–	–
Z_{start}	43%	36%	32%	87%	85%	–	26%
p_{450}	12%	–	34%	–	–	10%	26%

operation voltage V. Humidification of the membrane and the anode electrode sets in by product water until the current density reaches its peak plateau i_{peak}. The membrane reaches maximum protonic conductivity at $S_{q,peak,end}$. Now product water starts to decrease the surface of the porous electrodes and the current density drops down very fast. The level to which it drops down $i_{linear,start}$ is strongly dominated by the operating voltage V. Lower voltage is connected with higher waste heat production at the electrode resulting in a higher $i_{linear,start}$ because product water freezes in larger distance from the electrode.

This interpretation is supported by the fact that all charge transfer-related statements are highly influenced by the drying status of the cell whereas all current-related statements can be interpreted through heat production and are significantly influenced by the cell performance p_{450}, the cell voltage V and the air flow u_{air}.

Blockages of the gas channels by accumulated product water droplets would lead to higher pressure drops over the flowfield at constant gas flows. This is verified by comparisons of the pressure drop during fuel cell operation with and without (at V_{OC}) current production.

It is assumed that during cold start-up experiments with constant gas flows and stable pressure drop, most of the product water does not reach the flowfield channels, but freezes in the porous structures of the electrode, MPL and the GDL, which corresponds with the proposed mechanism presented in [4,5].

2.3. Electrochemical impedance spectroscopy

A single fuel cell with a double serpentine flowfield and an active area of 33 cm^2 was used for electrochemical impedance spectra (EIS) during isothermal, potentiostatic cold starts. Different frequency ranges were measured, applying an effective voltage excitation of ±5 mV (sine wave). The anode side (H_2) served as the reference electrode and was connected to the counter electrode. The cathode side (air) was connected to the working electrode. This set-up is also described in [6]. The upper frequency was 1000 Hz and the lower frequency varied between 0.1 and 0.04 Hz, because of the high dynamic behaviour of the current density over time. Since the current decay is fast, impedance spectra must be measured in a very short time otherwise the results show artefacts (fold back of the semicircle) at low frequencies, as the measuring time is inversely proportional to the applied frequency.

Fig. 3 shows an isothermal cold start experiment at −10 °C, constant gas flow rates of 150 ml min^{-1} air and 120 ml min^{-1} hydrogen. Ten EIS were applied in potentiostatic mode at 600 mV with an effective excitation of ±5 mV. The current density increases during the first three EIS within 1.5 min from 16 up to 38 mA cm^{-2}. EIS No. 4 and 5 were taken during the fast current decay between 2.5 and 7.5 min after starting the experiment. The measuring time for the following EIS No. 6 to EIS No. 10 was nearly 80 min, which means that the current decayed much slower and that it was more stable during EIS recording.

Fig. 4 shows 10 Nyquist plots of measured EIS during this cold start experiment. Next to the last measuring point the applied lowest frequency is printed. Assuming the simple electrode model of the cathode as suggested in [11] consisting of the membrane/contact resistance $R_{m,c}$ in series to the parallel charge transfer resistance R_{ct}, and the double-layer capacity C_d, one can estimate the values for $R_{m,c}$, which is addressed to the left basis point of the semicircle and R_{ct}, which represents the diameter of the semicircle in the Nyquist plot. The semicircles of EIS No. 1 and No. 5 show the abovementioned artefact in the last measuring point because the cell current was too unstable while EIS was recorded.

By linear regression analyses the most important influence parameters on the decrease of $R_{m,c}$ at the initial start of the experiment ($S_{q,cum} < 10$ C cm^{-2}) were identified. In Fig. 5, the result shows that $R_{m,c}$ decreases significantly with increasing

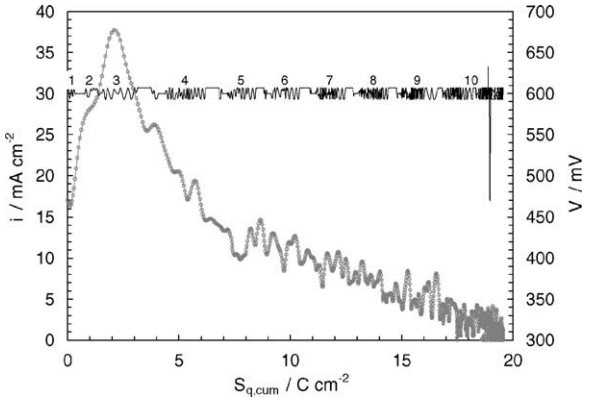

Fig. 3. Current density decay and operating voltage (600 mV ± 5 mV) of isothermal cold start-up at −10 °C, 150 ml min^{-1} air and 120 ml min^{-1} H_2. The voltage signal is modulated by the applied EIS frequency (1000–0.1 Hz/0.04 Hz) with an effective excitation of ±5 mV.

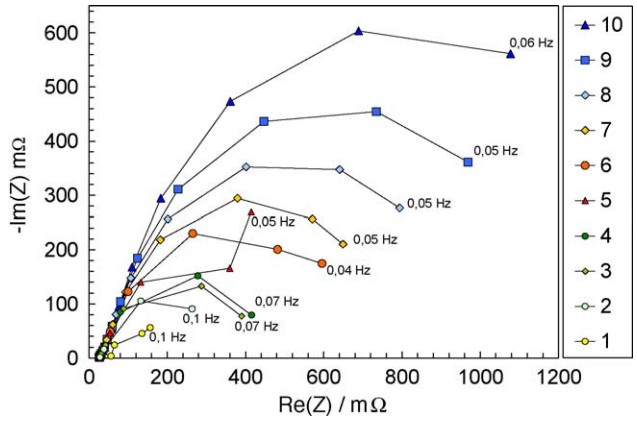

Fig. 4. Series of 10 EIS during a cold start-up experiment at 600 mV, 150 ml min^{-1} air and 120 ml min^{-1} H_2 flow. Frequency range of EIS between 1000 Hz and 40 mHz (lowest frequency is printed next to the last point). The voltage amplitude is ±5 mV.

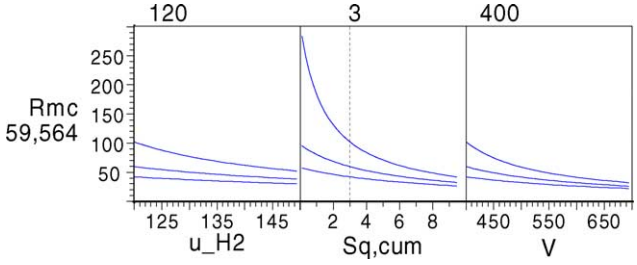

Fig. 5. Predicted membrane/contact resistance $R_{m,c}$ (mΩ) as function of the dominating three parameters. Linear regression of all experimental parameters ($R^2_{adj} = 0.75$).

$S_{q,cum}$. Higher operating voltage and hydrogen flow lead to lower $R_{m,c}$.

While there is a dependency between $R_{m,c}$ and the hydrogen flow one can find a significant influence of the air flow for the charge transfer resistance R_{ct}, which is mainly dominated by S_q. Fig. 6 illustrates the regression result for R_{ct} in a predicted response graph for all $S_{q,cum}$ higher than 10 C cm^{-2}.

Statistical evaluation of AC impedance spectra during isothermal cold start-up shows a strong dependency between the cumulated charge transfer density $S_{q,cum}$, the membrane/contact resistance $R_{m,c}$, and the charge transfer

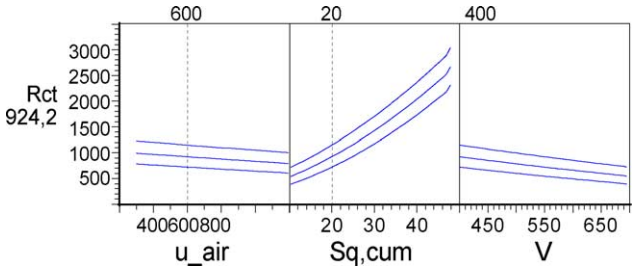

Fig. 6. Predicted charge transfer resistance R_{ct} (mΩ) as function of the dominating three operational parameters. Linear regression of all operational parameters ($R^2_{adj} = 0.83$).

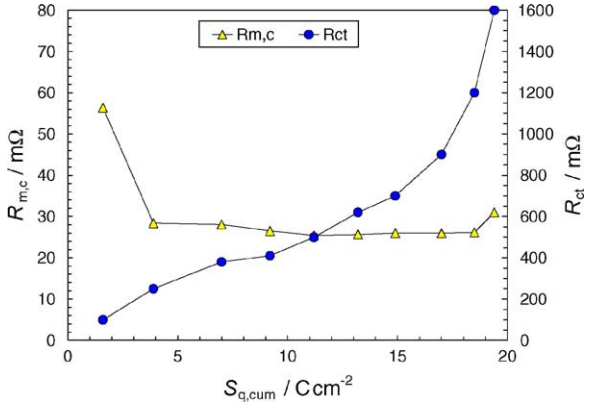

Fig. 7. Charge transfer resistance R_{ct} and membrane/contact resistance $R_{m,c}$ as function of the cumulated charge transfer density.

resistance R_{ct}. Fig. 7 illustrates the typical behaviour of both resistances during a cold start experiment.

Two effects support the shape of the current decay curves. At the initial start $R_{m,c}$ is high and stabilises later at a much lower level. As a result, the ohmic losses improve. This result confirms the formerly formulated assumption that the membrane gets humidified by product water even at sub zero temperatures. R_{ct} reacts converse; with longer experiment duration it increases and therefore the current density decays. This effect is addressed to a reduction of the active surface of the cathode electrode by ice formation.

2.4. Degradation effects

During several series of cold start experiments strong performance degradation at 450 mV was found. By cyclic voltammetry on the cathode side a decrease of the hydrogen desorption peak after 10 cold start-up experiments was observed as shown in Fig. 8. The anode side (flushed with H_2) served as the reference electrode and was connected to the counter electrode. The cathode side (flushed with N_2) was connected to the working electrode. After V_{OC} dropped

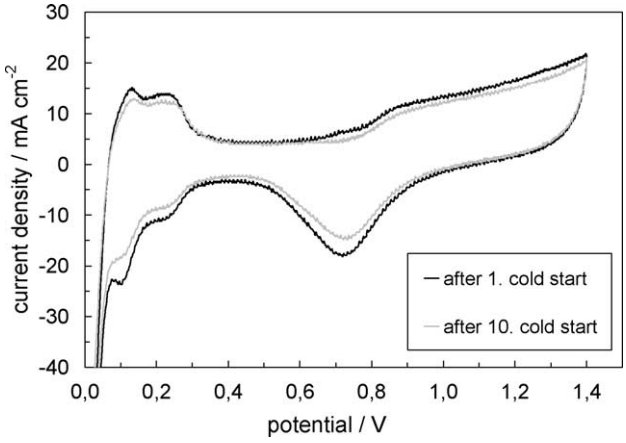

Fig. 8. Cyclic voltammograms after cold start-up experiment 1 and 10 with a scanning rate of 50 mV s^{-1}.

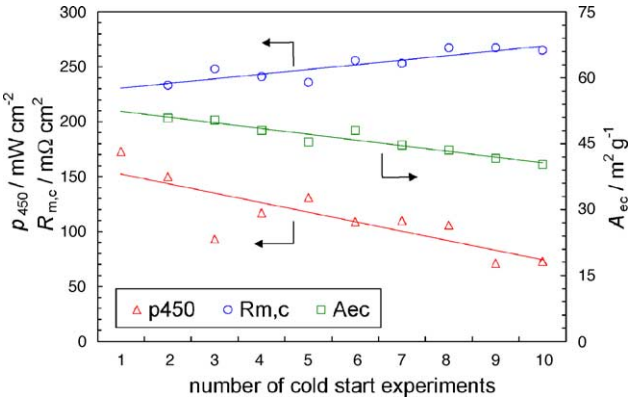

Fig. 9. Degradation of performance p_{450}, surface area A_{ec} and increase of membrane/contact resistance $R_{m,c}$ after 10 cold start experiments.

below 100 mV and stayed stable, the cell was cycled three times between 0 and 1.4 V with a scan rate of 50 mV s^{-1}.

The electrochemical active area A_{ec} can be estimated using the area of the hydrogen desorption peak, the scan rate and the specific charge for a hydrogen monolayer on platinum, which is 210 μC cm^{-2}. The fractional coverage of the hydrogen monolayer of 0.77 as proposed by Breiter et al. [12] is not included.

Fig. 9 illustrates all detected degradation effects during 10 cold start experiments for A_{ec}, the reference power density p_{450} and the high frequency membrane/contact resistance $R_{m,c}$ at the beginning of the cyclic voltammogram.

The decrease in the calculated electrochemical active surface A_{ec} from about 50 to 40 m^2 g^{-1} is connected with higher activation polarisation [6] and the increase in the high frequency resistance from 230 to 270 mΩ cm^2 does explain higher ohmic losses.

The average percentage changes per cold start-up are calculated in Table 4. The values are in the same range as reported in [6,9] and show that it is absolutely necessary to improve cold start and shut-down procedures to prevent performance degradation.

Table 4
Degradation by cold start experiments

Value	Unit	Change per cold start experiment
p_{450}	mW cm^{-2}	−5.4%
A_{ec}	m^2 g^{-1}	−2.4%
$R_{m,c}$	mΩ cm^2	+1.9%

After disassembling the cell it was found that the flowfield channel pattern is visible on the cathode GDL as dark lines (microscope image in Fig. 10a, magnification 3×). A hydrophobicity test showed that the channel pattern is much more hydrophilic (Fig. 10b) and water droplets agglomerate.

Ice formation could deform the pore structure in the MPL and the GDL. Oh et al. found by BET analysis after thermal cycles that the pore size distribution of the electrode changed to larger pores [6,9]. The same effect could occur in the MPL and the GDL. Other effects could also play a role, like washed-out, hydrophilic polymer chains of the membrane or loss of PTFE in the GDL.

To prove the loss of hydrophobicity in the GDL we performed contact angle measurements with 10 μl water droplets. Fig. 11 shows that the contact angle on the dark areas is about 112°, whereas on the not-coloured areas the contact angle is about 133°. On the anode side the same hydrophobicity test shows a uniform distribution and no channel pattern. The anode contact angle is 136° and comparable with hydrophobic parts of the cathode GDL. This indicates again that mainly the cathode is affected by ice formation during cold starts.

In this cell assembly also microporous layers were used, which are embedded by the MEA and the GDL. After disassembly of the cell it was found that the hydrophobicity of the cathode MPL has only changed. As well as on the cathode GDL water accumulated on the channel structure after the spray test. In Fig. 12, the channel pattern on the cathode MPL is visible by the agglomeration of water droplets. The image was taken under a microscope with a magnification of about 3×.

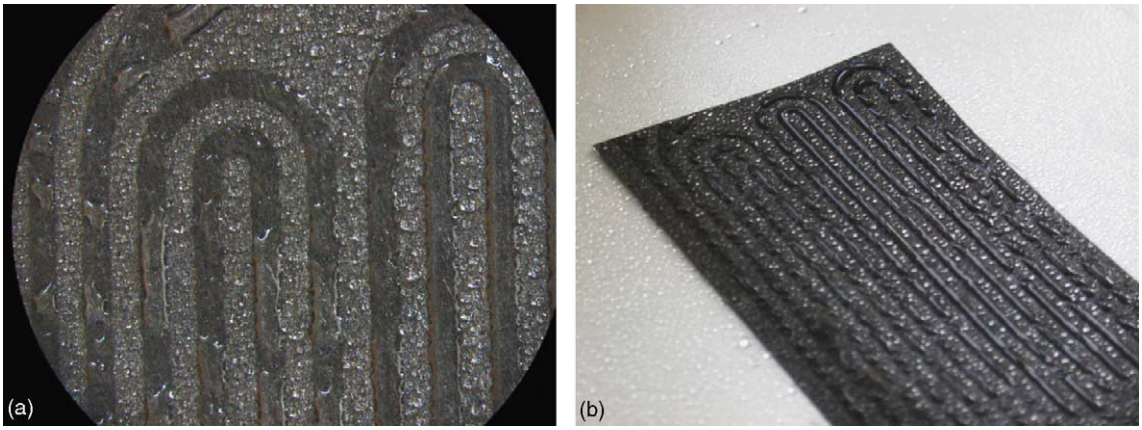

Fig. 10. Flowfield channel pattern on cathode GDL after cell disassembly and spray test with water. The hydrophilic channel pattern is visible.

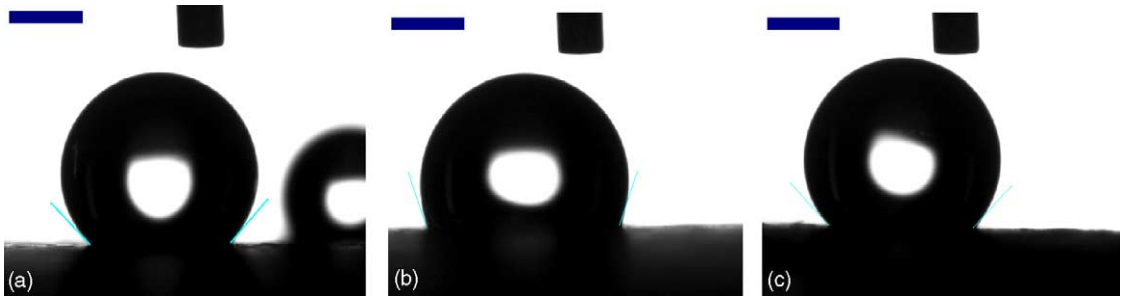

Fig. 11. Contact angle measurements with 10 μl water droplets. (a) uncoloured areas of cathode GDL (Ø = 133°), (b) coloured channel area of cathode GDL (Ø = 112°) and (c) anode GDL (Ø = 136°).

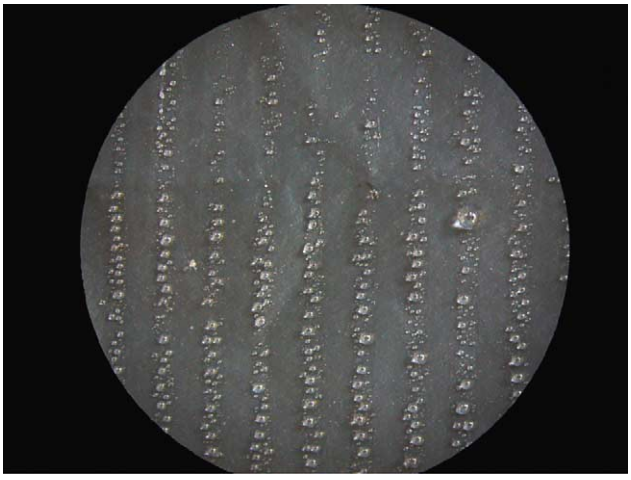

Fig. 12. Flowfield pattern on the microporous layer of the cathode. Water droplets cumulate in the more hydrophilic channel structure.

Further investigations to clarify the structural changes will be done by mercury porosimetry, BET analysis and SEM/EDS analyses.

3. Conclusions

By isothermal potentiostatic cold start measurements of single fuel cells under different operating conditions we found that water freezes in the porous structures of the cathode electrode, microporous layer, and the GDL. Statistic evaluation of the experiments showed that dryer membranes and high air flow rates are beneficial for high charge transfer rates. Furthermore, it was found that performance degradation plays an important role on the charge transfer too. As pre stage to physical models we presented statistic-based models which explain the characteristics of the current density during cold start-up as function of all operating parameters and estimates their significant influence. From these results we conclude that product water increases first the membrane humidity even at −10 °C, and after it has reached its maximum, product water floods the porous structures of the electrode, MPL and GDL, and freezes. Therefore, the current density decays. This assumption is proved by electrochemical impedance spectra during isothermal potentiostatic cold start experiments, which show that the membrane/contact resistance decreases, whereas the charge transfer resistance increases over time. For both values the charge transfer and the amount of product water, respectively, plays a significant role. Ice formation leads to a strong degradation of the cell performance and the electrochemical active surface area of the cathode. The membrane/contact resistance increases with the number of cold start-up experiments and structural changes on the cathode GDL and MPL were observed, leading to changes in hydrophobicity. To prevent degradation, elaborated start-up and shut-down procedures have to be developed in the future to overcome the obstacle cold start-up of PEM fuel cells.

References

[1] J. Cargnelli, P. Rivard, D. Frank, R.B. Gopal, Fuel cell for deployable applications in sub-zero environment, Portable Fuel Cells (1999).
[2] D. Chu, R. Jiang, K. Gardner, R. Jacobs, J. Schmidt, T. Quakenbush, J. Stephens, Polymer electrolyte membrane fuel cells for communication applications, J. Power Sources 96 (2001).
[3] B.K. Datta, G. Velayutham, A. Prasad Goud, Fuel cell power source for a cold region, J. Power Sources 106 (2002).
[4] F. Kagami; T. Ogawa; Y. Hishinuma; T. Chikahisa Simulating the performance of a PEFC at a temperature below freezing, Fuel cell seminar, Abstracts, 2002.
[5] F. Kagami, Y. Hishinuma, T. Chikahisa, Performance and self-starting of a PEFC at temperatures below freezing, Thermal Sci. Eng. 10 (3) (2002).
[6] EunAe Cho, Jae-Joon Ko, Heung Yong Ha, Seong-Ahn Hong, Characteristics of the PEMFC repetitively brought to temperatures below 0 °C, J. Electrochem. Soc. 150 (2003).
[7] R.C. McDonald, C.K. Mittelsteadt, E.L. Thompson, Proceedings of the 2nd European PEFC Forum on Freeze-Thaw Cycling of Proton-Exchange Membranes: Electrochemical and Mechanical Analyses, vol. 1, 2003.
[8] M. Cappadonia, J.W. Erning, U. Stimming, Proton conduction of Nafion 117 membrane between 140 K and room temperature, J. Electroanal. Chem. 376 (1994).
[9] In-Hwan Oh, EunAe Cho, Heung Yong Ha, Seong-Ahn Hong, Proceedings of the 2nd European PEFC Forum on Effect of Water Freezing on the Performance of PEMFC, vol. 1, 2003.
[10] K. Tüber Analyse des Betriebsverhaltens von Polymer-Membran-Brennstoffzellen für portable Systeme, Doctorate thesis; Uni-

versität Duisburg-Essen, 2004,;1; http://www.ub.uni-duisburg.de/ETD-db/theses/available/duett-10282004-143414/unrestricted/tueber_diss.pdf.
[11] C.H. Hamann, W. Vielstich, Elektrochemie, Wiley-VCH Verlag GmbH, 1975.
[12] M. Breiter, H. Kammermeier, C.A. Knorr, Z. Elektrochem. 60 (1956) 37.
[13] A. Handl: Statistik mit R; 2003. Fakultät für Wirtschaftswissenschaften; Universität Bielefeld, http://www.wiwi.uni-bielefeld.de/~frohn/Lehre/Statistik1/Skript/stat12b.pdf.